International Journal of Fatigue 127 (2019) 1–9

Contents lists available at ScienceDirect

International Journal of Fatigue

journal homepage: www.elsevier.com/locate/ijfatigue

Development of fatigue testing system for in-situ observation of stainless steel 316 by HS-AFM & SEM☆

Amir Farokh Payam[a,b,*], Oliver Payton[c], Loren Picco[d], Stacy Moore[c], Tomas Martin[c], A.D. Warren[c], Mahmoud Mostafavi[a], David Knowles[a]

[a] Solid Mechanics Research Group, Department of Engineering, University of Bristol, Bristol, UK
[b] School of Engineering, Ulster University, Newtownabbey, UK
[c] Interface Analysis Centre, HH Wills Physics Laboratory, University of Bristol, Bristol, UK
[d] Department of Physics, Virginia Commonwealth University, VA, USA

ARTICLE INFO

Keywords:
Fatigue
Fatigue initiation
SEM
HS-AFM
In-situ observation

ABSTRACT

A miniature three-point bend fatigue stage for in-situ observation of fatigue microcrack initiation and growth behaviour by scanning electron microscopy (SEM) and contact mode high-speed atomic force microscopy (HS-AFM) has been developed. Details of this stage are provided along with finite element simulations of the stress profiles of said stage and specimen on loading. The proposed stage facilitates study of the micro mechanisms of fatigue damage evolution when used during SEM and HS-AFM scanning of the sample surface. High amplitude low cycle fatigue tests have been carried out on annealed AISI Type 316 stainless steel to demonstrate the applicability of the system. Characteristic features of surface topography and evolution of slip bands observed have been documented. Images obtained by SEM and HS-AFM are presented for comparison. Finally, to demonstrate the capability of the new facility combined with HS-AFM, the spacing between slip bands and their height at different grains at the centre of the metal sample are measured and compared.

1. Introduction

Fatigue damage in the majority metallic systems requires the development of local reversed plasticity as a result of the application of repeated (cyclic) stresses; ultimately this leads to crack initiation [1]. There are three principal steps which may be observed in the fatigue process: initiation, including nucleation and micro growth, crack growth, and failure [2]. The first sign of fatigue damage which can lead to crack initiation in many metallic systems is slip band formation, evident on the polished surface of a stressed specimen [3]. These slip bands are the result of local plasticity on active slip systems and result in local elevations and depressions of the surface; generally termed surface extrusions and intrusions [4]. While several theoretical and computational methods have been proposed and developed to study fatigue crack initiation and growth, such as [5–15], physical evidence and validation data for fatigue nucleation, initiation and growth relies upon the development of experimental techniques and observations. Recent advances in modelling, such as crystal plasticity and dislocation dynamics approaches, have afforded the opportunity to model mesoscale plasticity in considerable detail. However due to the complexity of the local strain fields high resolution study at the grain and sub-grain level is required to validate the models rigorously. This information is critical to underpin and validate developments of current models, especially those focussing on nucleation and micro (early) growth stages [16]. Most historic observations of fatigue crack nucleation and growth have been performed by optical microscopy [11], limited transmission electron microscopy (TEM) [12] and/or scanning electron microscopy (SEM) [13–15]. Although notable insight has been obtained by these techniques, the fidelity of information on local plasticity was compromised by limited resolution of these microscopes and/or their inability to measure true sample topography.

Since 1994 [17] atomic force microscopy (AFM) has been used to study fatigue and to obtain quantitative information on slip spacings and slip height displacements of alloys under fully reversed plastic strain cycling. Several fatigue tests measurement have been performed by AFM for different alloys [11,15,17–37]. However, all such measurements suffer from significant time constraints associated with slow AFM scan which limits the quantification of slip bands during cyclic fatigue tests to very small areas [17,21,22,38]. Due to the low scanning speed of conventional AFMs, the scan size is rarely large enough to

☆ The background data published in the paper is available upon request by contacting the corresponding author.

* Corresponding author at: School of Engineering, Ulster University, Newtownabbey, UK.
E-mail address: a.farokh-payam@ulster.ac.uk (A.F. Payam).

https://doi.org/10.1016/j.ijfatigue.2019.05.015
Received 1 February 2019; Received in revised form 11 May 2019; Accepted 14 May 2019
Available online 15 May 2019
0142-1123/

accommodate significant grain numbers. Quantitative analyses are often limited to areas of the order of 10–15 μm^2.

In-situ and ex-situ bending tests have been used with AFM to study the effects of cyclic loading on slip accumulations [30,31,33,35]. In ex-situ experiments such as those reported in [31,35], the specimen were loaded cyclically by using a three point bending instrument and after removing the load; atomic force microscopy was used to scan the sample. As a consequence, during the measurement the specimens were not under load and the cycle by cycle observation of microcracks was not achievable due to effects such as closure of the microcrack faces. In-situ experiments, on the other hand, are based around development of bending fixtures that can be integrated with an AFM stage to allow observation of small fatigue crack growth under load [11,33]. The dynamic interaction of the in-situ loading frames, such as those used in SEMs with AFM stages has limited the sample size and even in such studies the maximum area that fatigue growth was investigated is of the order of 5 μm × 5 μm [11,33] which has not been big enough to consider the behaviour in more than a single grain. There is no quantification of slip width, height and spacing carried out in-situ in multi-grain materials. Such information is critical for the modelling community particularly those developing crystal plasticity models that incorporate the microstructure of the material in fatigue behaviour simulations and more importantly, prediction.

Design of a miniature bending fatigue testing machine which can be integrated with both commercial SEM and AFMs to provide the opportunity of in-situ observation of strain evolution and ultimately initiation and microcrack growth cycle by cycle is therefore a major evolution and focus our study. Critically it can provide information with high resolution (provided high speed measurement is available) of topography over a wide range of adjacent grains. To overcome the mentioned limitations and improve the possibility of fatigue study using SEM and AFM, for the first time we have designed and manufactured a miniature stage, which provide the ability of in-situ observation of cycle by cycle evolution of microcracks, slip bands, intrusions and extrusion while the specimen is under the load. Moreover, to overcome the limitation of quantitative analysis of fatigue initiation and growth by considering large images contain several grains, for the first time we demonstrate the application of high-speed AFM with angstrom resolution on local step height. The data from our measurements can be used to validate and calibrate crystal plasticity models, highlighting the stochastic nature of fatigue initiation which can be associated with the local shape, orientation and environment of individual grains. Informed models should then directly predict multi-axial behaviour without recourse to deformation rules such as equivalent stress or strain.

As a result of loading in the miniature stage, the surface relief formation in individual grains of annealed AISI Type 316 stainless steel with constant stress amplitude is presented and compared after 1000 and 10,000 cycles loading. The formation of slip bands at different regions of the specimen under low cycle three-point bending test is documented by SEM/HS-AFM and characteristic features of surface topography are measured by HS-AFM. The focus of the current work is evaluating the performance of the developed stage in conjunction with HS-AFM and to provide quantitative data in large scan area of several grains. The developed methodology can be used in future studies to quantify the evolution of slip bands and fatigue initiation in each cycle and open the door to much more detailed studies.

2. Materials and methods

2.1. Material and sample preparation

Cold rolled AISI Type 316 stainless steel plate 1 mm thick was used in this work with the nominal chemical composition provided in Table 1.

The stainless steel plate was cut into beams 20 × 6 × 1 mm in size to fit into the miniature stage (described below). The samples were annealed at 1050 °C for half an hour and cooled in air (giving a resultant proof stress of approximately 290 MPa). Preparation of the sample surface is critical for quantitative measurement from the HS-AFM and a suitable surface finish was achieved on the tensile face of the beam following the method outlined by Warren et al. [40]. The surface was initially polished using progressively finer grades of silicon carbide (SiC) grit paper, from P320, P800, P1200, P2400 to P4000, using water as lubricant. The sample was then polished using 1–0.25 μm diamond paste (Kemet International Ltd., KD Diamond Pastes), using a StruersTM DP-Lubricant (Brown). For the final polishing step, the sample was vibro-polished (VibroMetTM, Buehler) with colloidal silica (MasterMet R, Buehler) for 24 h.

To study the formation and growth of slip bands at the peak tensile stress region of the specimen and other selected tensile regions of the specimen, we marked locations on the sample using a focused ion beam (FIB). These fiducial marks enabled the same regions measured by HS-AFM and SEM to also be imaged by electron backscatter diffraction (EBSD) so that the plane orientation of the grains could be determined. The EBSD map was recorded at 1 μm step size using a Zeiss Sigma FEG-SEM with a 30 kV beam/125 μm aperture. The sample was mounted at 70 degrees to the beam, and the diffraction patterns were captured using a DigiView 3 high-speed camera. Data was collected in the most highly stress region using orientation image mapping (OIM) software (Ametek, Utah, USA). The results of which can be seen in Fig. 1.

2.2. Miniature-stage design

The miniature-stage was designed in a number of iterations, the most challenging task being to accommodate the limitations of the HS-AFM sample holder (size and weight). Geometrical aspects of the design were complemented with detailed stress analysis using FEA, to verify loading and deflection in both the specimen and stage itself. This latter aspect was found to be extremely important to determine the stage response under loading, and to prevent potential deformation and failure of the stage itself during testing. The stage was designed in such a way that, after cyclic loading, the sample can be maintained under a fixed load.

Details of the designed stage are illustrated in Fig. 2-a. The areas denoted A and B are related to the marked regions of the sample, subsequently analysed with the SEM and AFM. These are located at the point of maximum surface stress (centre) and 3 mm away from the centre of the sample where the surface stress has decayed to a substantially lower level. The finite element model (FEM) results from the Abaqus simulation are presented in Fig. 2-b. In the simulation, the force applied to the beam was set at 60 N, which resulted in a maximum displacement of the beam of just less than a 0.1 mm (0.092 mm) and a maximum stress at the top surface centre of the beam of 250 MPa. As seen in the simulation results, during the loading process, the resultant stress in the stage itself remains very low. The model consisted 4948 nodes and 3133 C3D20R reduced integration quadratic elements. The push rod was simulated using discrete rigid elements (C3D20R) with their motion associated with a reference point. The reference points were restricted in X and Y direction (see Fig. 2 for coordinate system) and the displacement was applied in the Z direction. Contact was defined between the rigid push rod and the rigid supports. The contact type is surface to surface full sliding with hard contact in normal direction and a 0.2 friction coefficient for tangential. Since the stresses at the contact point were not the subject of this study and the region of interest in the sample was far away from the contact point, this arrangement allowed for fast convergence of the simulation while providing a reasonable approximation for the effects of the loading instrumentation to be taken into account.

The stage, with integral loading points, was manufactured from EN24 steel by wire electro discharge machining. Images of the finished stage and how it fits into the loading machine and HS-AFM are given in

Table 1
Chemical composition (maxima unless range given) for stainless steel 316 (wt%), Fe balace [39]

Carbon	Manganese	Silicon	Chromium	Nickel	Molybdenum	Phosphorus	Sulphur	Nitrogen
0.08	2.00	0.75	16–18	10–14	2.0–3.0	0.045	0.03	0.1

Fig. 3. The loading machine used in our experiment was an Instron 1341 with a 1 kN load cell that is driven hydraulically. As shown in Fig. 3-c, the miniature stage is placed on the sample holder of Instron 1341 and loaded. Cyclic deformation tests were performed with 250 MPa peak surface stress (1000 and 10,000 cycles) in a three-point flexure bend approach. The three-point flexure fixture produces its peak stress at the specimen mid-point, with reduced stress elsewhere. The load was applied sinusoidally with a frequency of 2 Hz. Once the loading process was completed, the sample was locked and maintained under load. Then the stage could be moved to the SEM/HS-AFM for study, supported through the loading pin onto the stage. A schematic of the surface roughness induced by cyclic loading of our test is shown in Fig. 4 where P_{max} and P_{min} are the maximum and minimum loads applied to the specimen, respectively.

2.3. HS-AFM measurement

HS-AFM affords a major benefit over conventional AFM when considering fatigue as it is possible to rapidly image the deformed surface of the material with sub nanometre height resolution and nanometre lateral resolution, generating multiple megapixel frames per second. The imaging window of the HS-AFM can be translated, and data stitched across the surface to automatically map the sample at the length scales of multiple grains (in the material under investigation with average grain size 30 μm). In this study a contact mode HS-AFM (Bristol Nano Dynamics Ltd, UK) was employed [41,42] to gather data on the samples. Critically, the architecture of the system enabled enough height clearance for the micro-strain rig to be mounted in the microscope. Although the sample scanning nature of the tool dictates that the rig be light weight so as not to degrade the motions of the scanner.

The large area imaging mode of the HS-AFM allowed areas 100s μm in length to be explored in under an hour with no deterioration in lateral resolution; joystick control provided easy navigation of the sample in real-time to locate regions of interest. As HS-AFM, like all AFMs, measures the sample topography, it is possible to measure the true height of the slip bands on the surface with sub-atomic resolution (± 15 pm), which is less than the central spacing between closed pack atoms (analogous to one Burgers vector).

3. Results and discussion

Fig. 5 illustrates secondary electron SEM images of the annealed stainless steel plate before and after loading (10000 cycles) with a maximum stress of ~250 MPa at the centre of the beam (region A in Fig. 2-a) and ~120 MPa at the region B (Fig. 2-b) 3 mm away from the maximum stress location; the 0.2% proof stress of the material is 290 MPA. As can be seen from Fig. 5-c, at the centre of the sample (region A in Fig. 2-a), slip bands appeared in the grains while measurements taken 3 mm from the centre (region B at Fig. 2-a) show no clear evidence of slip banding (Fig. 5-b). Clearly the deformation at the centre of the specimen, although slightly below the large scale proof stress, produces larger strains which cause more slip bands in the centre region. When the sample is loaded, slip lines, related to local plastic deformation are evident as traces across the individual grains. Increasing the load clearly leads to the increase of the density and height of such slip lines. Fig. 5-c shows that at the centre of the specimen some grains have fully developed sets of slip bands, while the neighbouring grains have little surface deformation. This can be explained by the fact that the formation and development of slip bands at the grains strongly depends on the orientation of slip active system inside the grains relative to the applied major principal stress, somewhat modified by the neighbouring grain environment. So, based on the orientation of active slip systems towards the surface of material and the orientation of the trace of slip systems with loading axis, the formation and growth of slip bands at the grains are different.

HS-AFM characterises the surface morphology of the material and is insensitive to the phase. As such it cannot differentiate between a surface roughness caused by accumulated slip or due to stress induced phase transformation. The material used in this study, stainless steel 316L has an austenitic FCC structure which can show stress induced displacive martensitic phase transformation. The transformation of martensite can change the surface morphology similar to slip accumulation and HS-AFM cannot differentiated the two mechanisms from each other. However, there is conclusive evidence [43] that the displacive martensitic transformation of austenite is a function of stress and not accumulated plastic strain. As such, it can be expected that in a fatigue test, the transformations reach a steady state in the first half cycle when the maximum load is achieved. Any other change in the surface morphology after the first half cycle can then be attributed to slip accumulation i.e. an evolution of the accumulated local strain.

A 3D rendered HS-AFM topography maps of the sample with an area

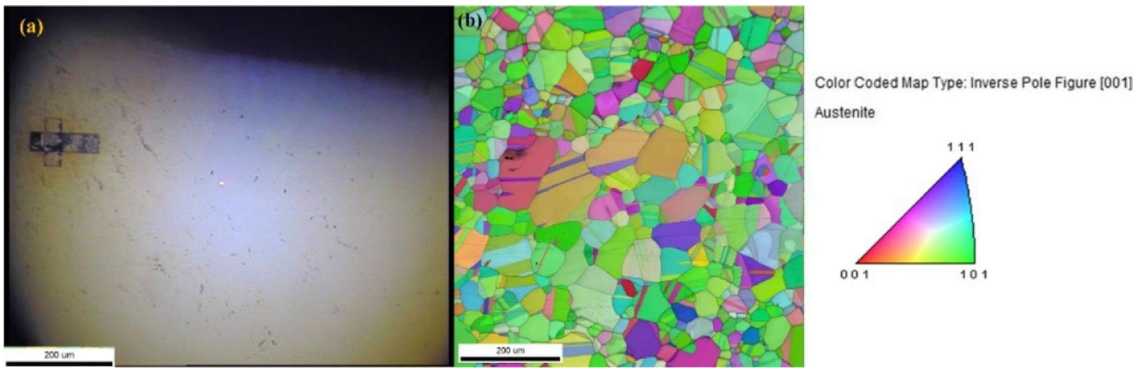

Fig. 1. (a) Optical image of the marked region of the centre showing the fiducial mark on the left, and the detection laser from the HS-AFM in the centre (cantilever chip moved out of focus) and (b) EBSD image of the centre part of the specimen.

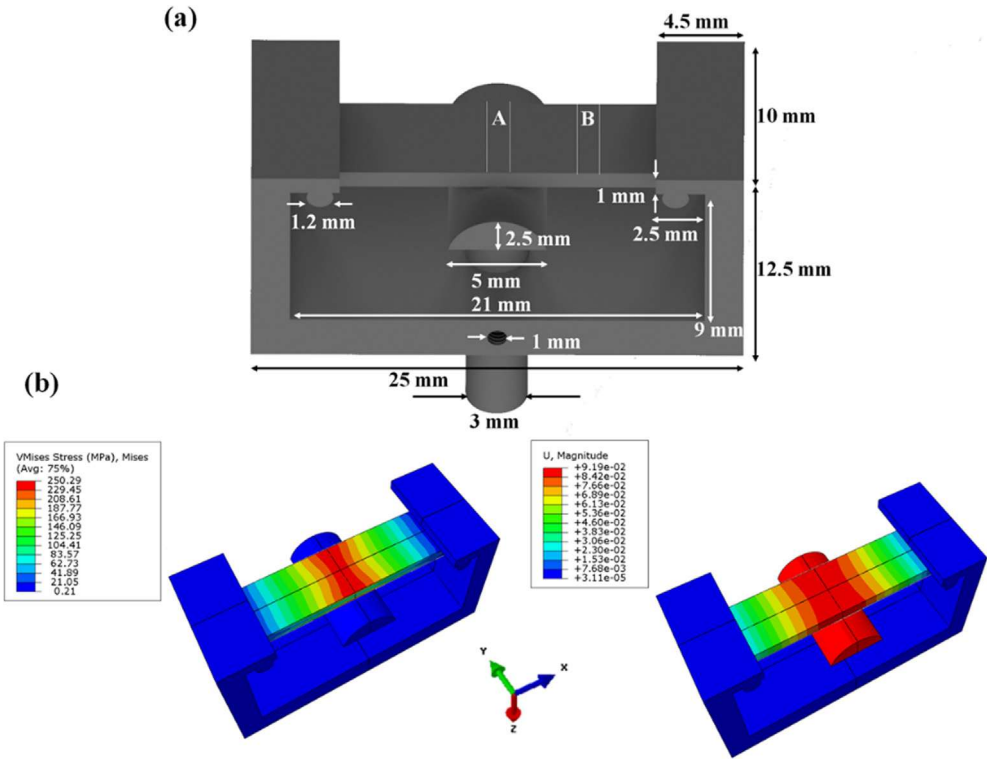

Fig. 2. (a) Schematic of the stage, (b) FEM simulation showing deformation, stress and minimal stress in the rig. Also, location of the fiducial marks and the stress at these points.

of 39 × 35 μm^2 and 42 × 27 μm^2 in region A following 1000 and 10,000 cycles are shown in Fig. 6. AISI type 316 stainless steel has a Face Centre Cubic crystallographic structure [32], therefore the slip planes are {1 1 1} [32]. As shown in Fig. 5-c and 6, in certain grains more than one slip plane is active; moving from one grain to another, there is clearly a change in the orientation of the slip plane evident consistent with the change in orientation of neighbouring grains. It is thus possible to distinguish different grains where there is a distinct change in the orientation of the parallel slip lines.

To analyse the slip height and separation of the slip bands in each grain, we studied individual HS-AFM frames from the composite maps shown in Fig. 6. In this preliminary study, we concentrated on three factors of fatigue damage evolution: (i) the slip height, (ii) the separation distance between slips, and (iii) the number of slip bands.

The quantitative results of the measured grains at the 39 × 35 μm^2 area of region A of the sample are presented in Figs. 7 and 8 and Table 2. Table 2 depicts the respective average value of slip height and separation distance between slips for the measured grains after 1000 and 10,000 loading cycles. After 1000 cycles loading, the height of slip bands varies between 0.25 nm and 8.5 nm with the average slip height at about 2.69 nm which is in the order of 10 Bürgers vectors translations. The average separation distance between slip bands is 2.3 μm. For the limited number of grains studied the probability distribution function map of slip heights and separation distances after 1000 cycles are shown in Fig. 7-a. As can be seen, the majority of slip band spacings are around 2.5–3 μm and the majority of slip heights are around 1.5–2 nm. The maximum observed slip height is 8.5 nm and minimum observable slip height is around 0.25 nm which is comparable with one Burgers vector translation. Recognising that the angle which the Burgers vector subtends relative to the surface plane normal has not been presented here. Fig. 7-b and c show two different frames of HS-AFM measurements from the 3d composite map of Fig. 6-a. Above a certain stress applied to the sample, more slip bands are activated in some grains due to the loading orientation (Fig. 7-b). This can be explained by the local stresses being high enough to release a new and more closely spaced slip bands [32]. Result of Fig. 7-c corresponds to another grain which consist of parallel slip bands. In this frame the slip separation distance is larger than Fig. 7-b.

The results of quantitative analysis from different frames of the measured grains for loading after 10,000 cycles are given in Fig. 8 and Table 2. The probability distribution function map of slip heights and separation distances are shown in Fig. 8-a. The single frame HS-AFM topography maps of a surface inside the measured grains after 10,000 cycles loading are shown in Fig. 8-b and c. The perpendicular orientations of slip plane bands can be seen in Fig. 8-b, with different height and separation. From Table 2 it is depicted that the average slip

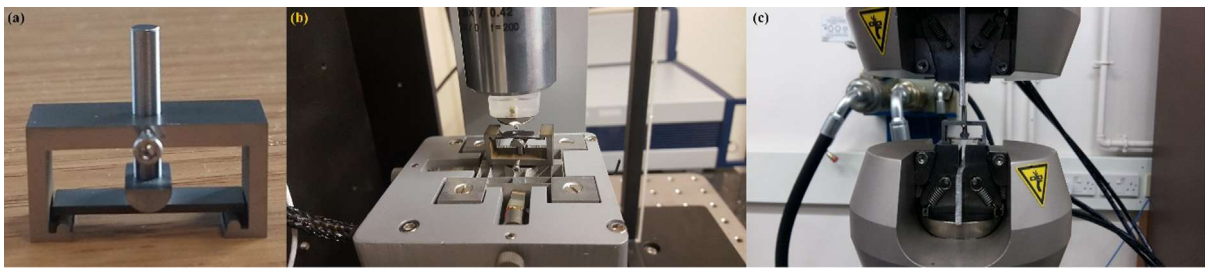

Fig. 3. Photos showing the rig (a) on its own, (b) in HS-AFM and (c) Loading rig.

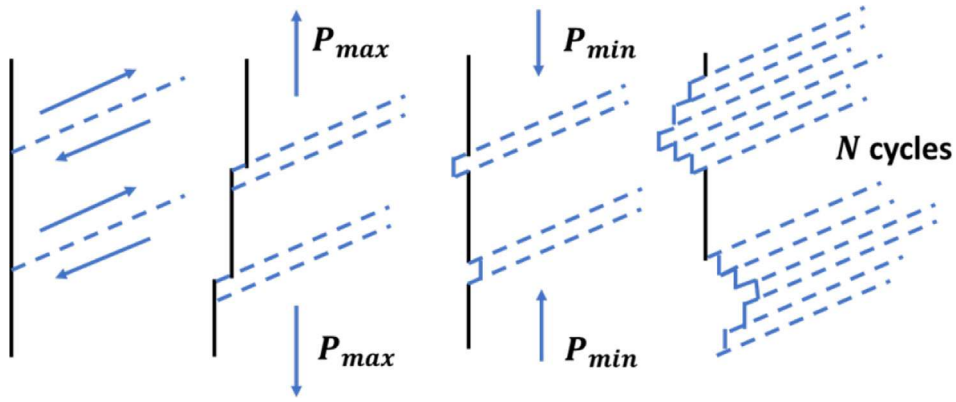

Fig. 4. Schematic of the surface roughness induced by cyclic loading.

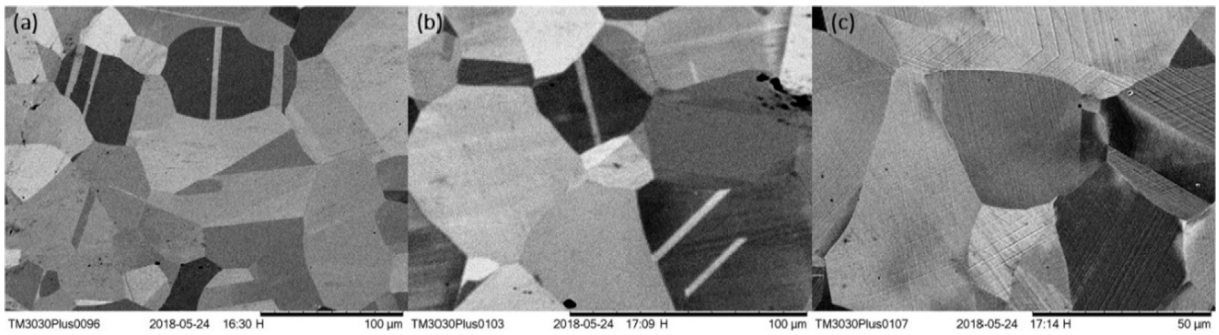

Fig. 5. Pre-loading SEM (a), post-loading SEM location of lower stress (b) and centre (c).

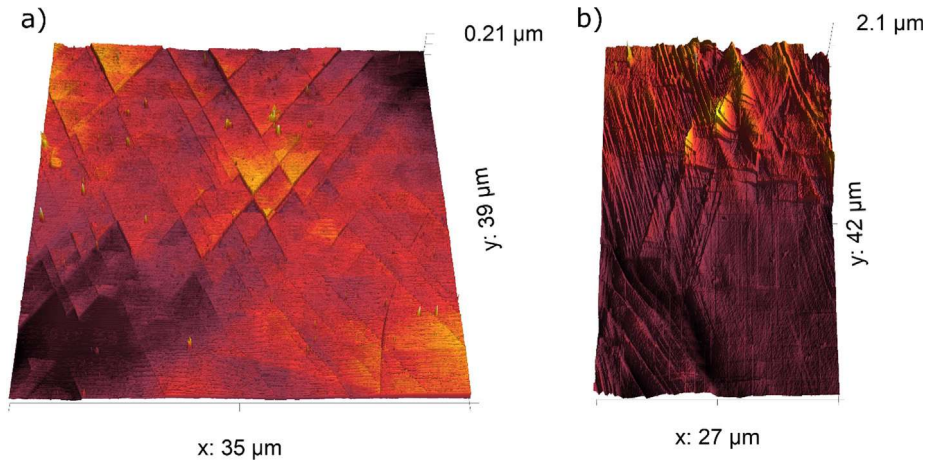

Fig. 6. Shows a composite 3d rendered HS-AFM topography map taken at region A of the sample after 1000 cycles loading (a) and nearby after 10,000 cycles (b). Significantly larger slip bands are observed after 10,000 cycles.

height after 10,000 cycle is 6.63 nm which means the average slip height after 10,000 cycles loading for maximum stress of 250 MPa is around 26 Bürgers vectors translations. The average slip distance is approximately 1 µm. After 10,000 cycles loading, due to strain accumulation, the number of slip bands is increased. Here, the quantitative analysis clearly shows the increase of the average slip height which can be associated to the growth of previously formed slip bands. For the 10,000 cycles condition, the maximum slip height is 43 nm and the minimum one is 0.25 nm. The minimum slip height is comparable with one Bürgers vector translation. In comparison with 1000 cycles loading, the average slip separation distance for the 10,000 cycles loading is decreased which is expected from the initiation and formation new slip bands between the existent slip bands produced in previous cycles. This means that during cyclic loading, which leads to the fatigue crack initiation, both the creation of new slip bands and an increase in irreversible plastic strain has occurred. This is illustrated by the results shown in Fig. 8-c (III) which consists of different slip heights.

Also, the visual interrogation of the frame shown in Fig. 8-b shows the presence of two perpendicular slip systems with different distance and height. Generally, based on the quantitative analysis of our measured images and data, it can be concluded that the greatest values of slip height are related to the slip bands which are initiated at the first cycles and grow by strain accumulation in subsequent cycles. The smaller slip height regions are related to the new initiated slips due to strain accumulation in higher cycles loading, for which there is an element of an initiation period. Here, due to the initiation and formation of new slips, the distribution and average of slip separation are decreased, which means the presence of more slips and formation of

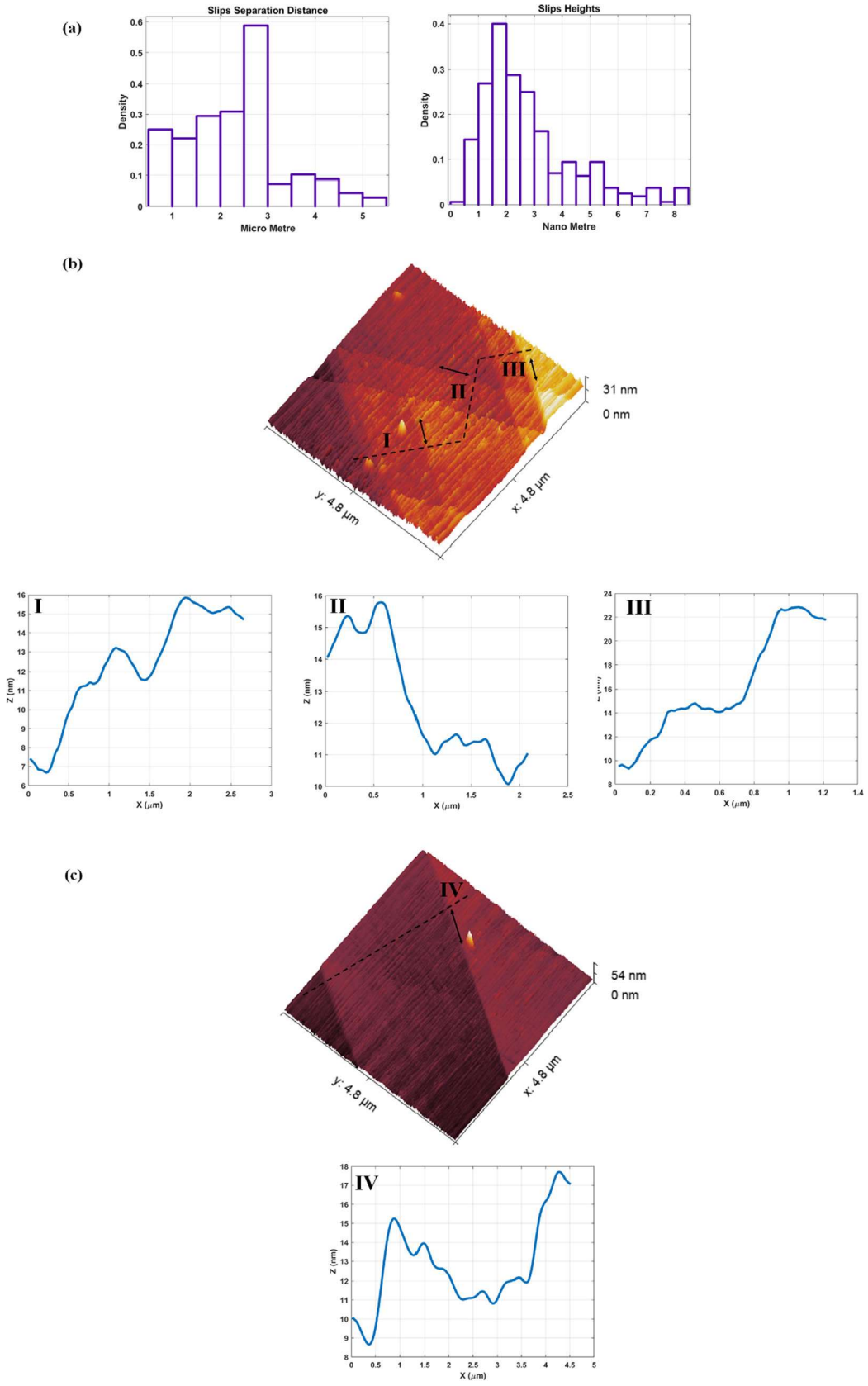

Fig. 7. Shows (a) probability distribution map of slips separation distance and height after 1000 cycles. HS-AFM topographic maps of the surface inside two different grains after 1000 cycles. The arrows indicate the trace of the slip planes: (b) different orientations. The profiles I, II and III taken along the lines I, II and III respectively show steps (c) 1 orientation. The profile IV taken along the line IV shows steps. The lines are started from left to right.

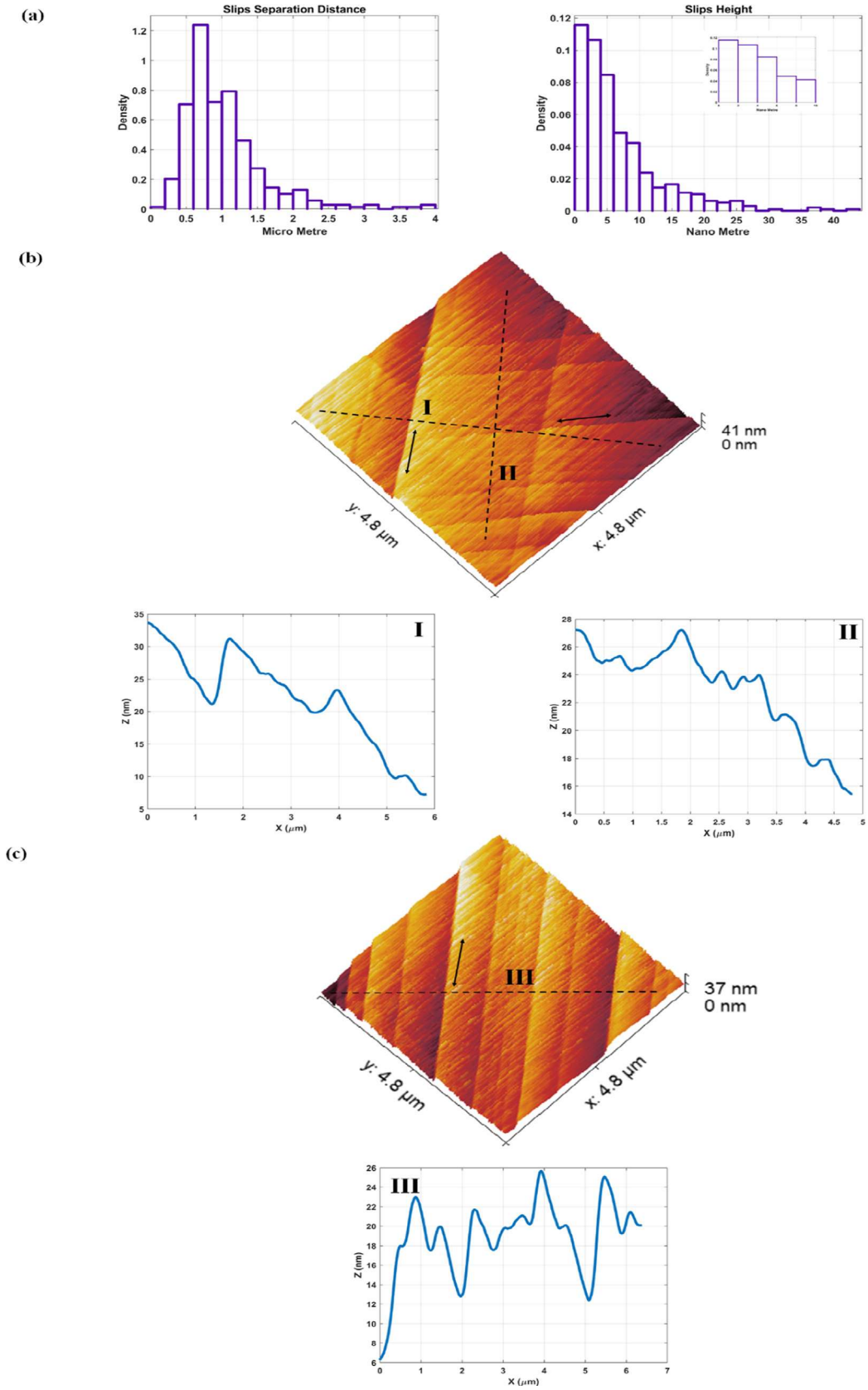

Fig. 8. Shows (a) probability distribution map of slips separation distance and height after 10,000 cycles. HS-AFM topographic maps of the surface inside different measured grains after 10,000 cycles as an illustrative example which have been used to generate data in (a). The arrows indicate the trace of the slip planes: (b) different orientations. The profiles I, II taken along the lines I and II respectively show steps (c) 1 orientation. The profile III taken along the line III shows steps. The lines are started from left to right.

Table 2
The mean, standard deviation and variance values of slip height and slip separation distance for measured grains under 1000 and 10,000 cycles loading with the applied stress range of 250 MPa.

	1000 Height (nm)	10,000 Height (nm)	1000 Separation (μm)	10,000 Separation (μm)
Mean	2.69	6.63	2.3	1
Standard Deviation	1.6761	6.551	1.0232	0.5742
Variance	2.8093	42.96	1.047	0.3297

slip parallel to the previous slip bands.

It is important to mention that the development of slip bands inside the grains is strongly dependant on the orientation of the active slip systems, which will be considered in our future study. In the current study, our first aim is to validate the performance of our designed miniature stage and show the capability of HS-AFM to provide topographic maps of large scan areas of the surface of specimen which consist of different grains. The second aim of our current study is to show the ability of HS-AFM to provide quantitative analysis of measured grains focusing on the number of slip bands, distribution and formation of slip heights and distances at different cycles of loading. To improve the comprehensiveness of quantification and analysis, the subsequent step will be the determination of the specific grain's orientation measured by EBSD and focus the HS-AFM measurements on the interested regions cycle by cycle. In this manner, based on the proposed methodology, the evolution of slip bands and initiation of fatigue in each cycle can be analysed, and the effect of grain orientations on the fatigue initiation/growth can be explored.

4. Conclusion

In this paper, we presented a miniature three-point bending fatigue testing stage for in-situ observation of microcrack initiation and growth behaviour by scanning electron microscopy (SEM) and contact mode high speed atomic force microscopy (HS-AFM). Using finite element analysis, the loading mechanism with the proposed stage is simulated and the stress concentration on the surface of the specimen is analysed. Then, the constructed stage is used to study in-situ the fatigue behaviour of annealed AISI type 316 stainless steel. The SEM results of the surface before and after the loading shows good agreement with finite element simulations.

For the first time, HS-AFM has been used to interrogate areas containing several grains, potentially unlocking the historical limitation of conventional AFM. HS-AFM provided a unique opportunity for in-situ observation of initiation and growth of multiple cracks over a substantial number of grains without a need for artificially introducing crack initiation sites (e.g. stress risers such as notches). The information which the HS-AFM technique can provide, quantifying intrusions/extrusion and slip band cycle by cycle over a number of grains, therefore represents a major change to the data available to calibrate and validate mesoscale-models; at a length scale which is appropriate to the underlying constitutive relations (that describe grain to grain strain variation and damage evolution). A second major differentiator of HS-AFM technique is the ability to interrogate the stochastic nature of strain and damage evolution – sampling a wide range of grain sizes, orientations and local environments in a single experiment. This again is essential for mesoscale model development which is cognisant of the underlying variation in the material at a grain level.

Acknowledgment

The authors would like to acknowledge the support provided by EPSRC under grant number EP/R020108/1 and University of Bristol's Strategic Grant. We are grateful to Mr. Dimitris Samaras and Mr. Freddie Russell-Pavier for their assistance in HS-AFM measurements and Mr. Satyajit Day for fruitful discussions about Abaqus.

References

[1] Schijve Jaap. Fatigue of structures and materials. Dordrecht: Springer; 2009.
[2] Milella PP. Fatigue and corrosion in metals. Springer-Nature; 2013.
[3] Buffiere J-Y. Fatigue crack initiation and propagation from defects in metals: Is 3D characterization important? Procedia Struct Integr 2017;7:27–32.
[4] Man J, Obrtlík K, Polák J. Extrusions and intrusions in fatigued metals. Part 1. State of the art and history. Philos Mag 2009;89(16):1295–336.
[5] Déprés C, Robertson CF, Fivel MC. Low-strain fatigue in 316L steel surface grains: a three dimension discrete dislocation dynamics modelling of the early cycles. Part 2: Persistent slip markings and micro-crack nucleation. Philos Mag 2006;86(1):79–97.
[6] Merah N, Saghir F, Khan Z, Bazoune A. A study of frequency and temperature effects on fatigue crack growth resistance of CPVC. Eng Fract Mech 2005;72(11):1691–701.
[7] Hosseini ZS, Dadfarnia M, Somerday BP, Sofronis P, Ritchie RO. On the theoretical modeling of fatigue crack growth. J Mech Phys Solids 2018;121:341–62.
[8] Zhang Z, Lunt D, Abdolvand H, Wilkinson AJ, Preuss M, Dunne FPE. Quantitative investigation of micro slip and localization in polycrystalline materials under uniaxial tension. Int J Plast 2018;108:88–106. December 2017.
[9] Zheng Z, Stapleton A, Fox K, Dunne FPE. Understanding thermal alleviation in cold dwell fatigue in titanium alloys. Int J Plast 2018;111:234–52. https://doi.org/10.1016/j.ijplas.2018.07.018.
[10] Guery A, Hild F, Latourte F, Roux S. Slip activities in polycrystals determined by coupling DIC measurements with crystal plasticity calculations. Int J Plast 2016;81:249–66.
[11] A. Ueno, H. Kishimoto, "Development of in situ observation fatigue testing systems and their application, in Fatigue," in Proceedings of the Seventh International Fatigue Congress, Vol. 4/4.
[12] Huang JY, Yeh JJ, Jeng SL, Chen CY, Kuo RC. High-cycle fatigue behavior of type 316L stainless steel. Mater Trans 2006;47(2):409–17.
[13] Wilkinson AJ, Ben Britton T. "Strains, planes, and EBSD in materials science". Mater Today 2012;15(9):366–76.
[14] Barrios A, Gupta S, Castelluccio GM, Pierron ON. Quantitative in situ SEM high cycle fatigue: the critical role of oxygen on nanoscale-void-controlled nucleation and propagation of small cracks in Ni microbeams. Nano Lett 2018;18(4):2595–602.
[15] Biallas G, Maier HJ. In-situ fatigue in an environmental scanning electron microscope - potential and current limitations. Int J Fatigue 2007;29(8):1413–25.
[16] Man J, Klapetek P, Man O, Weidner A, Obrtlík K, Polák J. Extrusions and intrusions in fatigued metals. Part 2. AFM and EBSD study of the early growth of extrusions and intrusions in 316L steel fatigued at room temperature. Philos Mag 2009;89(16):1337–72.
[17] Harvey SE, Marsh PG, Gerberich WW. Atomic force microscopy and modeling of fatigue crack initiation in metals. Acta Metall Mater 1994;42(10):3493–502.
[18] Man J, Valtr M, Kuběna I, Petrenec M, Obrtlík K, Polák J. AFM and FIB study of cyclic strain localization and surface relief evolution in fatigued f.c.c. polycrystals. Adv Mater Res 2014;891–892:524–9.
[19] Oda Y, Furuya Y, Noguchi H, Higashida K. AFM and SEM observation on mechanism of fatigue crack growth in an Fe-Si single crystal. Int J Fract 2002;113(3):213–31.
[20] Man J, et al. AFM and SEM-FEG study on fundamental mechanisms leading to fatigue crack initiation. Int J Fatigue 2015;76:11–8.
[21] Cretegny L, Saxena A. AFM characterization of the evolution of surface deformation during fatigue in polycrystalline copper. Acta Mater. 2001;49(18):3755–65.
[22] Polák J, Man J, Obrtlík K. AFM evidence of surface relief formation and models of fatigue crack nucleation. Int J Fatigue 2003;25(9–11):1027–36.
[23] Kramer DE, Savage MF, Levine LE. AFM observations of slip band development in Al single crystals. Acta Mater 2005;53(17):4655–64.
[24] Man J, Valtr M, Weidner A, Petrenec M, Obrtlk K, Polk J. AFM study of surface relief evolution in 316L steel fatigued at low and high temperatures. Procedia Eng 2010;2(1):1625–33.
[25] Jono M, Sugeta A, Uematsu Y. Atomic force microscopy and the mechanism of fatigue crack growth. Fatigue Fract Eng Mater Struct 2001;24(12):831–42.
[26] Schwab A, Meißner O, Holste C. Atomic force microscopy of slip lines on the surface of a fatigued nickel single crystal. Philos Mag Lett 1998;77(1):23–31.
[27] Liu H, Bhushan B. Bending and fatigue study on a nanoscale hinge by an atomic force microscope. Nanotechnology 2004;15(9):1246–51.
[28] Yoshikazu N, Manabu K, Shohei H. Characterization of fatigue crack initiation condition of steels with afm. ICF XI - 11th Int. Conf Fract 2005.
[29] Payam Amir Farokh, Payton Oliver, Mostafavi Mahmoud, Picco Loren, Moore Stacy, Martin Tomas, Warren AD. Development of fatigue testing system for in-situ observation by AFM & SEM. ICMFF12. 2019.
[30] Sugeta A, Uematsu Y, Tomita K, Hirose K, Jono M. Development of fatigue testing

system for in-situ observation by an atomic force microscope and small fatigue crack growth behavior in.ALPHA.-brass. Trans Japan Soc Mech Eng Ser A 2011;70(692):588–95.
[31] Man J, Klapetek P, Man O, Weidner A, Obrtlík K, Polák J. Extrusions and intrusions in fatigued metals. Part 2. AFM and EBSD study of the early growth of extrusions and intrusions in 316L steel fatigued at room temperature. Philos Mag 2009;89(16):1337–72.
[32] Martin FA, Cousty J, Bataillon C. In situ AFM study of pitting corrosion and corrosion under strain on a 304L stainless steel. Congr Proc EUROCORR 2004;16(12):1–10.
[33] Sugeta A, Uematsu Y. In-situ atomic force microscopy and crystallo graphic orientation analysis of small fatigue crack deflection behavior. Key Eng Mater 2009;345–346:227–30.
[34] Nakai Y, Fukuhara S, Ohnishi K. Observation of fatigue damage in structural steel by scanning atomic force microscopy. Int J Fatigue 2002;19(93):223–36.
[35] Xie JJ, Wu XL, Hong YS. Study on fatigue crack nucleation of electrodeposited nanocrystalline nickel. Adv Mater Res 2009;33–37:925–30.
[36] Cretegny L, Saxena A. "Use of Atomic Force Microscopy in Assessing Surface". *ICF10* Honolulu Hawaii - 2001 2001.
[37] Risbet M, Feaugas X, Guillemer-Neel C, Clavel M. Use of atomic force microscopy to quantify slip irreversibility in a nickel-base superalloy. Scr Mater 2003;49(6):533–8.
[38] Fathi Sola J, Kelton R, Meletis EI, Huang H. A surface roughness based damage index for predicting future propagation path of microstructure-sensitive crack in pure nickel. Int J Fatigue 2019;122:164–72. https://doi.org/10.1016/j.ijfatigue.2019.01.012.
[39] Sandmeyer Steel, "Specification Sheet: Alloy 316/316L," no. 1, p. 3, 2014.
[40] Warren AD, Martinez-Ubeda AI, Payton OD, Picco L, Scott TB. Preparation of stainless steel surfaces for scanning probe microscopy. Micros Today 2016;24(03):52–5.
[41] Laferrere A, et al. In situ imaging of corrosion processes in nuclear fuel cladding. Corros Eng Sci Technol 2017;52(8):596–604.
[42] Moore S, et al. A study of dynamic nanoscale corrosion initiation events by HS-AFM. Faraday Discuss 2018.
[43] Das A, Chakraborti PC, Tarafder S, Bhadeshia HKDH. Analysis of deformation induced martensitic transformation in stainless steels. Mater Sci Technol 2011;27(1):366–70.